Research Article | Vol. 24, No. 20 | 3 Oct 2016 | OPTICS EXPRESS 22469
Optics EXPRESS

X-ray absorption spectroscopy using a self-seeded soft X-ray free-electron laser

THOMAS KROLL,[1,2] JAN KERN,[1,3] MARKUS KUBIN,[4] DANIEL RATNER,[1] SHERAZ GUL,[3] FRANKLIN D. FULLER,[3] HEIKE LÖCHEL,[5] JACEK KRZYWINSKI,[1] ALBERTO LUTMAN,[1] YUANTAO DING,[1] GEORGI L. DAKOVSKI,[1] STEFAN MOELLER,[1] JOSHUA J. TURNER,[1] ROBERTO ALONSO-MORI,[1] DENNIS L. NORDLUND,[2] JENS REHANEK,[5,6] CHRISTIAN WENIGER,[4] ALEXANDER FIRSOV,[5] MARIA BRZHEZINSKAYA,[5] RUCHIRA CHATTERJEE,[3] BENEDIKT LASSALLE-KAISER,[7] RAYMOND G. SIERRA,[1,8] HARTAWAN LAKSMONO,[8] ETHAN HILL,[9] ANDREW BOROVIK,[9] ALEXEI ERKO,[5] ALEXANDER FÖHLISCH,[4,10] ROLF MITZNER,[4] VITTAL K. YACHANDRA,[3,13] JUNKO YANO,[3,12] PHILIPPE WERNET,[4,11] AND UWE BERGMANN,[1,8,*]

[1]*Linac Coherent Light Source, SLAC National Accelerator Laboratory, Menlo Park, California 94025, USA*
[2]*Stanford Synchrotron Radiation Lightsource, SLAC National Accelerator Laboratory, Menlo Park, California 94025, USA*
[3]*Molecular Biophysics and Integrated Bioimaging Division, Lawrence Berkeley National Laboratory, Berkeley, California 94720, USA*
[4]*Institute for Methods and Instrumentation for Synchrotron Radiation Research, Helmholtz-Zentrum Berlin für Materialien und Energie GmbH, 12489 Berlin, Germany*
[5]*Institute for Nanometer Optics and Technology, Helmholtz-Zentrum Berlin für Materialien und Energie, 12489 Berlin, Germany*
[6]*Paul-Scherrer-Institut, 5232 Villigen-PSI, Switzerland*
[7]*Synchrotron SOLEIL, L'Orme des Merisiers, Saint-Aubin - BP 48, 91192 GIF-SUR-YVETTE Cedex, France*
[8]*Stanford PULSE Institute, SLAC National Accelerator Laboratory, Menlo Park, CA 94025, USA*
[9]*Department of Chemistry, University of California-Irvine, 1102 Natural Sciences II, Irvine, California 92697, USA*
[10]*Institut für Physik und Astronomie, Universität Potsdam Karl-Liebknecht-Strasse 24/25, 14476 Potsdam, Germany*
[11]*wernet@helmholtz-berlin.de*
[12]*jyano@lbl.gov*
[13]*vkyachandra@lbl.gov*
[*]*bergmann@slac.stanford.edu*

Abstract: X-ray free electron lasers (XFELs) enable unprecedented new ways to study the electronic structure and dynamics of transition metal systems. L-edge absorption spectroscopy is a powerful technique for such studies and the feasibility of this method at XFELs for solutions and solids has been demonstrated. However, the required x-ray bandwidth is an order of magnitude narrower than that of self-amplified spontaneous emission (SASE), and additional monochromatization is needed. Here we compare L-edge x-ray absorption spectroscopy (XAS) of a prototypical transition metal system based on monochromatizing the SASE radiation of the linac coherent light source (LCLS) with a new technique based on self-seeding of LCLS. We demonstrate how L-edge XAS can be performed using the self-seeding scheme without the need of an additional beam line monochromator. We show how the spectral shape and pulse energy depend on the undulator setup and how this affects the x-ray spectroscopy measurements.

OCIS codes: (340.7480) X-rays, soft x-rays, extreme ultraviolet (EUV); (340.0340) X-ray optics; (300.6560) Spectroscopy, x-ray; (050.2770) Gratings; (000.1570) Chemistry; (000.2190) Experimental physics.

#267761 http://dx.doi.org/10.1364/OE.24.022469
Journal © 2016 Received 6 Jun 2016; revised 18 Aug 2016; accepted 26 Aug 2016; published 19 Sep 2016

Optics EXPRESS

References and links

1. C. Bostedt, S. Boutet, D. M. Fritz, Z. Huang, H. J. Lee, H. T. Lemke, A. Robert, W. F. Schlotter, J. J. Turner, and G. J. Williams, "Linac Coherent Light Source: The first five years," Rev. Mod. Phys. **88**(1), 015007 (2016).
2. H. T. Lemke, C. Bressler, L. X. Chen, D. M. Fritz, K. J. Gaffney, A. Galler, W. Gawelda, K. Haldrup, R. W. Hartsock, H. Ihee, J. Kim, K. H. Kim, J. H. Lee, M. M. Nielsen, A. B. Stickrath, W. Zhang, D. Zhu, and M. Cammarata, "Femtosecond x-ray absorption spectroscopy at a hard x-ray free electron laser: Application to spin crossover dynamics," J. Phys. Chem. A **117**(4), 735–740 (2013).
3. T. Kubacka, J. A. Johnson, M. C. Hoffmann, C. Vicario, S. de Jong, P. Beaud, S. Grübel, S.-W. Huang, L. Huber, L. Patthey, Y.-D. Chuang, J. J. Turner, G. L. Dakovski, W.-S. Lee, M. P. Minitti, W. Schlotter, R. G. Moore, C. P. Hauri, S. M. Koohpayeh, V. Scagnoli, G. Ingold, S. L. Johnson, and U. Staub, "Large-amplitude spin dynamics driven by a THz pulse in resonance with an electromagnon," Science **343**(6177), 1333–1336 (2014).
4. W. Zhang, R. Alonso-Mori, U. Bergmann, C. Bressler, M. Chollet, A. Galler, W. Gawelda, R. G. Hadt, R. W. Hartsock, T. Kroll, K. S. Kjær, K. Kubiček, H. T. Lemke, H. W. Liang, D. A. Meyer, M. M. Nielsen, C. Purser, J. S. Robinson, E. I. Solomon, Z. Sun, D. Sokaras, T. B. van Driel, G. Vankó, T.-C. Weng, D. Zhu, and K. J. Gaffney, "Tracking excited-state charge and spin dynamics in iron coordination complexes," Nature **509**(7500), 345–348 (2014).
5. P. Wernet, K. Kunnus, I. Josefsson, I. Rajkovic, W. Quevedo, M. Beye, S. Schreck, S. Grübel, M. Scholz, D. Nordlund, W. Zhang, R. W. Hartsock, W. F. Schlotter, J. J. Turner, B. Kennedy, F. Hennies, F. M. F. de Groot, K. J. Gaffney, S. Techert, M. Odelius, and A. Föhlisch, "Orbital-specific mapping of the ligand exchange dynamics of $Fe(CO)_5$ in solution," Nature **520**(7545), 78–81 (2015).
6. M. Dell'Angela, F. Hieke, F. Sorgenfrei, N. Gerken, M. Beye, N. Gerasimova, H. Redlin, and W. Wurth, "Ultrafast surface dynamics probed with time resolved photoemission," Surf. Sci. **643**, 197–202 (2016).
7. D. Milathianaki, S. Boutet, G. J. Williams, A. Higginbotham, D. Ratner, A. E. Gleason, M. Messerschmidt, M. M. Seibert, D. C. Swift, P. Hering, J. Robinson, W. E. White, and J. S. Wark, "Femtosecond visualization of lattice dynamics in shock-compressed matter," Science **342**(6155), 220–223 (2013).
8. E. F. Garman and M. Weik, "Radiation damage to macromolecules: kill or cure?" J. Synch. Radiat. **22**(2), 195–200 (2015).
9. J. Kern, R. Alonso-Mori, R. Tran, J. Hattne, R. J. Gildea, N. Echols, C. Glöckner, J. Hellmich, H. Laksmono, R. G. Sierra, B. Lassalle-Kaiser, S. Koroidov, A. Lampe, G. Han, S. Gul, D. Difiore, D. Milathianaki, A. R. Fry, A. Miahnahri, D. W. Schafer, M. Messerschmidt, M. M. Seibert, J. E. Koglin, D. Sokaras, T.-C. Weng, J. Sellberg, M. J. Latimer, R. W. Grosse-Kunstleve, P. H. Zwart, W. E. White, P. Glatzel, P. D. Adams, M. J. Bogan, G. J. Williams, S. Boutet, J. Messinger, A. Zouni, N. K. Sauter, V. K. Yachandra, U. Bergmann, and J. Yano, "Simultaneous femtosecond x-ray spectroscopy and diffraction of photosystem II at room temperature," Science **340**(6131), 491–495 (2013).
10. S. Schreck, M. Beye, J. A. Sellberg, T. McQueen, H. Laksmono, B. Kennedy, S. Eckert, D. Schlesinger, D. Nordlund, H. Ogasawara, R. G. Sierra, V. H. Segtnan, K. Kubicek, W. F. Schlotter, G. L. Dakovski, S. P. Moeller, U. Bergmann, S. Techert, L. G. M. Pettersson, P. Wernet, M. J. Bogan, Y. Harada, A. Nilsson, and A. Föhlisch, "Reabsorption of soft x-ray emission at high x-ray free-electron laser fluences," Phys. Rev. Lett. **113**(15), 153002 (2014).
11. R. Alonso-Mori, J. Kern, R. J. Gildea, D. Sokaras, T.-C. Weng, B. Lassalle-Kaiser, R. Tran, J. Hattne, H. Laksmono, J. Hellmich, C. Glöckner, N. Echols, R. G. Sierra, D. W. Schafer, J. Sellberg, C. Kenney, R. Herbst, J. Pines, P. Hart, S. Herrmann, R. W. Grosse-Kunstleve, M. J. Latimer, A. R. Fry, M. M. Messerschmidt, A. Miahnahri, M. M. Seibert, P. H. Zwart, W. E. White, P. D. Adams, M. J. Bogan, S. Boutet, G. J. Williams, A. Zouni, J. Messinger, P. Glatzel, N. K. Sauter, V. K. Yachandra, J. Yano, and U. Bergmann, "Energy-dispersive X-ray emission spectroscopy using an x-ray free-electron laser in a shot-by-shot mode," Proc. Natl. Acad. Sci. U.S.A. **109**(47), 19103–19107 (2012).
12. F. Bencivenga, R. Cucini, F. Capotondi, A. Battistoni, R. Mincigrucci, E. Giangrisostomi, A. Gessini, M. Manfredda, I. P. Nikolov, E. Pedersoli, E. Principi, C. Svetina, P. Parisse, F. Casolari, M. B. Danailov, M. Kiskinova, and C. Masciovecchio, "Four-wave mixing experiments with extreme ultraviolet transient gratings," Nature **520**(7546), 205–208 (2015).
13. K. C. Prince, E. Allaria, C. Callegari, R. Cucini, G. De Ninno, S. Di Mitri, B. Diviacco, E. Ferrari, P. Finetti, D. Gauthier, L. Giannessi, N. Mahne, G. Penco, O. Plekan, L. Raimondi, P. Rebernik, E. Roussel, C. Svetina, M. Trovò, M. Zangrando, M. Negro, P. Carpeggiani, M. Reduzzi, G. Sansone, A. N. Grum-Grzhimailo, E. V. Gryzlova, S. I. Strakhova, K. Bartschat, N. Douguet, J. Venzke, D. Iablonskyi, Y. Kumagai, T. Takanashi, K. Ueda, A. Fischer, M. Coreno, F. Stienkemeier, Y. Ovcharenko, T. Mazza, and M. Meyer, "Coherent control with a short-wavelength free-electron laser," Nat. Photonics **10**(3), 176–179 (2016).
14. J. Zaanen, G. A. Sawatzky, J. Fink, W. Speier, and J. C. Fuggle, "$L_{2,3}$ absorption spectra of the lighter 3d transition metals," Phys. Rev. B Condens. Matter **32**(8), 4905–4913 (1985).
15. S. P. Cramer, F. M. F. de Groot, Y. Ma, C. T. Chen, F. Sette, C. A. Kipke, D. M. Eichhorn, M. K. Chan, W. H. Armstrong, E. Libby, G. Christou, S. Brooker, V. Mckee, O. C. Mullins, and J. C. Fuggle, "Ligand field strengths and oxidation states from manganese L-edge spectroscopy," J. Am. Chem. Soc. **113**(21), 7937–7940 (1991).

Optics EXPRESS

16. J. van Elp, J. L. Wieland, H. Eskes, P. Kuiper, G. A. Sawatzky, F. M. F. de Groot, and T. S. Turner, "Electronic structure of CoO, Li-doped CoO, and $LiCoO_2$," Phys. Rev. B Condens. Matter **44**(12), 6090–6103 (1991).
17. M. W. Haverkort, Z. Hu, J. C. Cezar, T. Burnus, H. Hartmann, M. Reuther, C. Zobel, T. Lorenz, A. Tanaka, N. B. Brookes, H. H. Hsieh, H.-J. Lin, C. T. Chen, and L. H. Tjeng, "Spin state transition in $LaCoO_3$ studied using soft x-ray absorption spectroscopy and magnetic circular dichroism," Phys. Rev. Lett. **97**(17), 176405 (2006).
18. T. Kroll, R. Kraus, R. Schönfelder, V. Yu. Aristov, O. V. Molodtsova, P. Hoffmann, and M. Knupfer, "Transition metal phthalocyanines: Insight into the electronic structure from soft x-ray spectroscopy," J. Chem. Phys. **137**(5), 054306 (2012).
19. S. A. Wilson, T. Kroll, R. A. Decreau, R. K. Hocking, M. Lundberg, B. Hedman, K. O. Hodgson, and E. I. Solomon, "Iron L-edge X-ray absorption spectroscopy of oxy-picket fence porphyrin: Experimental insight into Fe-O_2 bonding," J. Am. Chem. Soc. **135**(3), 1124–1136 (2013).
20. T. Katayama, T. Anniyev, M. Beye, R. Coffee, M. Dell'Angela, A. Föhlisch, J. Gladh, S. Kaya, O. Krupin, A. Nilsson, D. Nordlund, W. F. Schlotter, J. A. Sellberg, F. Sorgenfrei, J. J. Turner, W. Wurth, H. Öström, and H. Ogasawara, "Ultrafast soft x-ray emission spectroscopy of surface adsorbates using an x-ray free electron laser," J. Electron Spectrosc. Relat. Phenom. **187**, 9–14 (2013).
21. M. Dell'Angela, T. Anniyev, M. Beye, R. Coffee, A. Föhlisch, J. Gladh, T. Katayama, S. Kaya, O. Krupin, J. LaRue, A. Møgelhøj, D. Nordlund, J. K. Nørskov, H. Öberg, H. Ogasawara, H. Oström, L. G. M. Pettersson, W. F. Schlotter, J. A. Sellberg, F. Sorgenfrei, J. J. Turner, M. Wolf, W. Wurth, and A. Nilsson, "Real-time observation of surface bond breaking with an X-ray laser," Science **339**(6125), 1302–1305 (2013).
22. M. Beye, T. Anniyev, R. Coffee, M. Dell'Angela, A. Föhlisch, J. Gladh, T. Katayama, S. Kaya, O. Krupin, A. Møgelhøj, A. Nilsson, D. Nordlund, J. K. Nørskov, H. Öberg, H. Ogasawara, L. G. M. Pettersson, W. F. Schlotter, J. A. Sellberg, F. Sorgenfrei, J. J. Turner, M. Wolf, W. Wurth, and H. Oström, "Selective ultrafast probing of transient hot chemisorbed and precursor states of CO on Ru(0001)," Phys. Rev. Lett. **110**(18), 186101 (2013).
23. H. Öström, H. Öberg, H. Xin, J. LaRue, M. Beye, M. Dell'Angela, J. Gladh, M. L. Ng, J. A. Sellberg, S. Kaya, G. Mercurio, D. Nordlund, M. Hantschmann, F. Hieke, D. Kühn, W. F. Schlotter, G. L. Dakovski, J. J. Turner, M. P. Minitti, A. Mitra, S. P. Moeller, A. Föhlisch, M. Wolf, W. Wurth, M. Persson, J. K. Nørskov, F. Abild-Pedersen, H. Ogasawara, L. G. M. Pettersson, and A. Nilsson, "Probing the transition state region in catalytic CO oxidation on Ru," Science **347**(6225), 978–982 (2015).
24. R. Mitzner, J. Rehanek, J. Kern, S. Gul, J. Hattne, T. Taguchi, R. Alonso-Mori, R. Tran, C. Weniger, H. Schröder, W. Quevedo, H. Laksmono, R. G. Sierra, G. Han, B. Lassalle-Kaiser, S. Koroidov, K. Kubicek, S. Schreck, K. Kunnus, M. Brzhezinskaya, A. Firsov, M. P. Minitti, J. J. Turner, S. Moeller, N. K. Sauter, M. J. Bogan, D. Nordlund, W. F. Schlotter, J. Messinger, A. Borovik, S. Techert, F. M. F. de Groot, A. Föhlisch, A. Erko, U. Bergmann, V. K. Yachandra, P. Wernet, and J. Yano, "L-edge X-ray absorption spectroscopy of dilute systems relevant to metalloproteins using an X-ray free-electron laser," J. Phys. Chem. Lett. **4**(21), 3641–3647 (2013).
25. S. E. Canton, K. S. Kjær, G. Vankó, T. B. van Driel, S. Adachi, A. Bordage, C. Bressler, P. Chabera, M. Christensen, A. O. Dohn, A. Galler, W. Gawelda, D. Gosztola, K. Haldrup, T. Harlang, Y. Liu, K. B. Møller, Z. Németh, S. Nozawa, M. Pápai, T. Sato, T. Sato, K. Suarez-Alcantara, T. Togashi, K. Tono, J. Uhlig, D. A. Vithanage, K. Wärnmark, M. Yabashi, J. Zhang, V. Sundström, and M. M. Nielsen, "Visualizing the non-equilibrium dynamics of photoinduced intramolecular electron transfer with femtosecond x-ray pulses," Nat. Commun. **6**, 6359 (2015).
26. B. Erk, R. Boll, S. Trippel, D. Anielski, L. Foucar, B. Rudek, S. W. Epp, R. Coffee, S. Carron, S. Schorb, K. R. Ferguson, M. Swiggers, J. D. Bozek, M. Simon, T. Marchenko, J. Küpper, I. Schlichting, J. Ullrich, C. Bostedt, D. Rolles, and A. Rudenko, "Imaging charge transfer in iodomethane upon x-ray photoabsorption," Science **345**(6194), 288–291 (2014).
27. P. Emma, R. Akre, J. Arthur, R. Bionta, C. Bostedt, J. Bozek, A. Brachmann, P. Bucksbaum, R. Coffee, F.-J. Decker, Y. Ding, D. Dowell, S. Edstrom, A. Fisher, J. Frisch, S. Gilevich, J. Hastings, G. Hays, Ph. Hering, Z. Huang, R. Iverson, H. Loos, M. Messerschmidt, A. Miahnahri, S. Moeller, H.-D. Nuhn, G. Pile, D. Ratner, J. Rzepiela, D. Schultz, T. Smith, P. Stefan, H. Tompkins, J. Turner, J. Welch, W. White, J. Wu, G. Yocky, and J. Galayda, "First lasing and operation of an ångstrom-wavelength free-electron laser," Nat. Photonics **4**(9), 641–647 (2010).
28. D. P. Bernstein, Y. Acremann, A. Scherz, M. Burkhardt, J. Stöhr, M. Beye, W. F. Schlotter, T. Beeck, F. Sorgenfrei, A. Pietzsch, W. Wurth, and A. Föhlisch, "Near edge x-ray absorption fine structure spectroscopy with x-ray free-electron lasers," Appl. Phys. Lett. **95**(13), 134102 (2009).
29. P. Heimann, O. Krupin, W. F. Schlotter, J. Turner, J. Krzywinski, F. Sorgenfrei, M. Messerschmidt, D. Bernstein, J. Chalupský, V. Hájková, S. Hau-Riege, M. Holmes, L. Juha, N. Kelez, J. Lüning, D. Nordlund, M. F. Perea, A. Scherz, R. Soufli, W. Wurth, and M. Rowen, "Linac Coherent Light Source soft x-ray materials science instrument optical design and monochromator commissioning," Rev. Sci. Instrum. **82**(9), 093104 (2011).
30. W. F. Schlotter, J. J. Turner, M. Rowen, P. Heimann, M. Holmes, O. Krupin, M. Messerschmidt, S. Moeller, J. Krzywinski, R. Soufli, M. Fernández-Perea, N. Kelez, S. Lee, R. Coffee, G. Hays, M. Beye, N. Gerken, F. Sorgenfrei, S. Hau-Riege, L. Juha, J. Chalupsky, V. Hajkova, A. P. Mancuso, A. Singer, O. Yefanov, I. A. Vartanyants, G. Cadenazzi, B. Abbey, K. A. Nugent, H. Sinn, J. Lüning, S. Schaffert, S. Eisebitt, W. S. Lee, A. Scherz, A. R. Nilsson, and W. Wurth, "The soft X-ray instrument for materials studies at the Linac coherent light source X-ray free-electron laser," Rev. Sci. Instrum. **83**(4), 043107 (2012).

Optics EXPRESS

31. G. L. Dakovski, P. Heimann, M. Holmes, O. Krupin, M. P. Minitti, A. Mitra, S. Moeller, M. Rowen, W. F. Schlotter, and J. J. Turner, "The soft X-ray research instrument at the Linac coherent light source," J. Synchrotron Radiat. **22**(3), 498–502 (2015).
32. S. Moeller, G. Brown, G. Dakovski, B. Hill, M. Holmes, J. Loos, R. Maida, E. Paiser, W. Schlotter, J. J. Turner, A. Wallace, U. Jastrow, S. Kreis, A. A. Sorokin, and K. Tiedtke, "Pulse energy measurement at the SXR instrument," J. Synchrotron Radiat. **22**(3), 606–611 (2015).
33. K. Tiedtke, A. A. Sorokin, U. Jastrow, P. Juranić, S. Kreis, N. Gerken, M. Richter, U. Arp, Y. Feng, D. Nordlund, R. Soufli, M. Fernández-Perea, L. Juha, P. Heimann, B. Nagler, H. J. Lee, S. Mack, M. Cammarata, O. Krupin, M. Messerschmidt, M. Holmes, M. Rowen, W. Schlotter, S. Moeller, and J. J. Turner, "Absolute pulse energy measurements of soft x-rays at the Linac Coherent Light Source," Opt. Express **22**(18), 21214–21226 (2014).
34. D. Ratner, R. Abela, J. Amann, C. Behrens, D. Bohler, G. Bouchard, C. Bostedt, M. Boyes, K. Chow, D. Cocco, F. J. Decker, Y. Ding, C. Eckman, P. Emma, D. Fairley, Y. Feng, C. Field, U. Flechsig, G. Gassner, J. Hastings, P. Heimann, Z. Huang, N. Kelez, J. Krzywinski, H. Loos, A. Lutman, A. Marinelli, G. Marcus, T. Maxwell, P. Montanez, S. Moeller, D. Morton, H. D. Nuhn, N. Rodes, W. Schlotter, S. Serkez, T. Stevens, J. Turner, D. Walz, J. Welch, and J. Wu, "Experimental demonstration of a soft x-ray self-seeded free-electron laser," Phys. Rev. Lett. **114**(5), 054801 (2015).
35. R. Soufli, M. Fernández-Perea, S. L. Baker, J. C. Robinson, E. M. Gullikson, P. Heimann, V. V. Yashchuk, W. R. McKinney, W. F. Schlotter, and M. Rowen, "Development and calibration of mirrors and gratings for the soft x-ray materials science beamline at the Linac Coherent Light Source free-electron laser," Appl. Opt. **51**(12), 2118–2128 (2012).
36. K. Kunnus, I. Rajkovic, S. Schreck, W. Quevedo, S. Eckert, M. Beye, E. Suljoti, C. Weniger, C. Kalus, S. Grübel, M. Scholz, D. Nordlund, W. Zhang, R. W. Hartsock, K. J. Gaffney, W. F. Schlotter, J. J. Turner, B. Kennedy, F. Hennies, S. Techert, P. Wernet, and A. Föhlisch, "A setup for resonant inelastic soft x-ray scattering on liquids at free electron laser light sources," Rev. Sci. Instrum. **83**(12), 123109 (2012).
37. R. G. Sierra, H. Laksmono, J. Kern, R. Tran, J. Hattne, R. Alonso-Mori, B. Lassalle-Kaiser, C. Glöckner, J. Hellmich, D. W. Schafer, N. Echols, R. J. Gildea, R. W. Grosse-Kunstleve, J. Sellberg, T. A. McQueen, A. R. Fry, M. M. Messerschmidt, A. Miahnahri, M. M. Seibert, C. Y. Hampton, D. Starodub, N. D. Loh, D. Sokaras, T.-C. Weng, P. H. Zwart, P. Glatzel, D. Milathianaki, W. E. White, P. D. Adams, G. J. Williams, S. Boutet, A. Zouni, J. Messinger, N. K. Sauter, U. Bergmann, J. Yano, V. K. Yachandra, and M. J. Bogan, "Nanoflow electrospinning serial femtosecond crystallography," Acta Crystallogr. D Biol. Crystallogr. **68**(11), 1584–1587 (2012).
38. C. Braig, H. Löchel, R. Mitzner, W. Quevedo, P. Loukas, M. Kubin, C. Weniger, A. Firsov, J. Rehanek, M. Brzhezinskaya, P. Wernet, A. Föhlisch, and A. Erko, "Design and optimization of a parallel spectrometer for ultra-fast X-ray science," Opt. Express **22**(10), 12583–12602 (2014).
39. R. Lindberg, ANL tech. note AOP-TN-2015–028 (2015).
40. Z. Zhang, R. Lindberg, W. M. Fawley, Z. Huang, I. Krzywinski, A. Lutman, G. Marcus, and A. Marinelli, "Microbunching-instability-induced sidebands in a seeded free-electron laser," Phys. Rev. Accel. Beams **19**, 050701 (2016).

1. Introduction

X-ray Free Electron Lasers (XFELs) are unique sources for the study of electronic and atomic structure and dynamics, dramatically extending the capabilities of synchrotron radiation (SR) sources, which have been at the center of such studies over the past several decades [1]. The ultra-bright femtosecond (fs) x-ray pulses produced at XFELs allow not only the studies of ultrafast dynamics [2–6] and materials in extreme short-lived conditions [7], but also they can probe a sample faster than the onset of x-ray damage [8–11]. The seeded FERMI FEL at Elettra Synchrotron Trieste, Italy (~12-300 eV) also allows well-controlled experiments based on nonlinear techniques [12] and coherent control [13] mainly in the vacuum ultraviolet (VUV) spectral region.

To study the electronic structure of complexes such as catalysts, metalloenzymes, bio-inspired materials, and correlated electron systems, x-ray absorption spectroscopy (XAS), in particular in the soft x-ray regime, is a powerful tool. Prominent examples in the soft x-ray regime are 3d transition metal L-edge and ligand K-edge XAS, with their high sensitivity to oxidation and spin states, and the potential to extract the order of orbital energy levels, the symmetry and the covalency of the studied complexes [14–19]. These methods have been successfully applied to date at synchrotrons, and they are being established at XFELs to investigate ultrafast dynamics in chemical reactions on surfaces [20–23], in liquids [3,4,24,25] and gases [26].

Optics EXPRESS

In standard operation, LCLS delivers a beam of x-ray pulses generated by the self-amplified spontaneous emission (SASE) process [27], where the pulses have a relative spectral width of the order of 0.5%. Soft x-ray L- and K-edge XAS in the 250-1000 eV range typically require a spectral resolution corresponding to 0.05%, hence the beam has to be passed through a grating monochomator (~20% reflectivity) with a bandwidth- narrowing exit slit, although it has been shown that at ~100 eV experiments without an exit slit can be performed [28]. As a consequence of these and related losses in typical soft x-ray beamlines, the monochromatic peak flux on the sample at the soft x-ray endstation (SXR) of LCLS is reduced to a few percent of the original peak flux depending on the selected resolving power [29–33]. This reduced monochromatic photon flux is a limitation in particular for L-edge absorption spectroscopy of 3d transition metal atoms for dilute samples such as metalloenzymes (~mM) and for more complex techniques that require a particularly high average flux such as inelastic x-ray scattering (RIXS) measurements that hold great potential for quantitative electronic structure analyses [4].

To address these limitations imposed by the SASE process for soft x-ray spectroscopy applications, a new soft x-ray self-seeding mode of operation has been demonstrated and implemented recently at the LCLS [34]. In self-seeding, the monochromatization is performed before the laser amplification. As a consequence, one can obtain a higher spectral brightness as compared to SASE where the monochromatization is done post lasing [34]. For this, the FEL is split into two FELs and a monochromatic beam generated by passing the first FEL through a grating monochromator is used to (self) seed the second FEL. The amplification in the second FEL thus starts from a well-characterized seed and the losses in the grating monochromator in the first FEL proceed the amplification in the second FEL. One can therefore expect an improvement for soft x-ray spectroscopy applications by a narrower bandwidth and a higher peak and average flux in the self-seeded mode of LCLS compared to the SASE mode, as discussed in the body of the paper.

In this paper we test this hypothesis by explicitly investigating the feasibility of XAS when using the soft x-ray self-seeded mode of operation of the LCLS. With XAS at the L absorption edge of a dilute solution of a 3d transition metal Mn sample, we address in detail the influence of changes in resolving power, wavelength stability, peak and average flux when going from SASE to the self-seeded mode. In addition, we investigate how spurious effects in the self-seeded mode such as backgrounds caused by competing SASE growth and distortions to the seeded wavelength due to a non-ideal electron beam affect the XAS results. We close with an outlook towards using seeding schemes for soft x-ray XAS and RIXS and their time-resolved versions and the potential use of seeded FELs for non-linear variants of these methods.

2. Methods

2.1 Experimental setup

Data collection of the partial fluorescence yield (PFY) measurements were performed at the SXR instrument at the LCLS [29–33,35] as described by Mitzner et al. in [24]. A schematic drawing of the set up including the self-seeding scheme of the FEL is depicted in Fig. 1. $MnCl_2$ aqueous solution samples (500 mM) were injected into the x-ray beam in the liquid jet end station (LJE) [36] by means of an electrohydrodynamic-focused liquid jet of several micrometers in diameter in the cone-jet mode [37]. PFY data were collected by either using the SASE pulse and a grating monochromator, or pulses produced with the self-seeding setup. In the first case, the incoming energy is scanned by the beam line monochromator, while in the latter case the seeded mode monochromator is scanned (see below). The x-ray pulses had a duration of ~100 fs at a repetition rate of 120 Hz. The number of photons per pulse on the sample and the spectral width of the pulses depends on the operation mode of LCLS and the beamline settings as will be discussed below. A Kirkpatrick-Baez optics system was used to produce a beam size of 70 (v) x 30 (h) μm^2 at the sample. The PFY signal was detected using

Optics EXPRESS

a reflection zone-plate (RZP) spectrometer with an energy bandwidth of 20 eV, (Fig. 1) [24,38] where for the first time a new-generation 3-dimensional laterally depth-graded RZP was implemented. Using a RZP allows to discriminate the O K emission from the Mn L emission especially for systems in aqueous solutions [24]. In addition, it allows a clean determination of I_0 through its zero-order reflection. Two 2-dimensional CCD cameras (iKon-L 936, Andor Ltd., UK) were used to integrate the dispersed fluorescence from the sample as well as the zero-order reflection from the zone plates for each energy point while scanning a XAS spectrum. The CCD cameras were cooled to −60°C in order to decrease thermal noise. Integration time per energy point was 10 seconds, images were corrected for background signals as discussed below, and normalized to the total fluorescence signal given by the zero-order signal in the CCD images. The scanning range and step size are visible in Fig. 4.

The synchrotron fluorescence data of 500 µm $MnCl_2$ in H_2O run in a GDVN jet, were recorded using the RZP spectrometer with same settings as above at beam line U41_PGM at Bessy II with a photon flux of 8.8^{12} photons/second and a beam size of 100 (v) x 50 (h) μm^2 at the sample. The bandwidth defined by the monochromator exit slit opening of 40 µm was $\Delta E = 450$ meV.

2.2 Soft X-ray self-seeding

Operating LCLS in the standard SASE scheme leads to a spectral bandwidth of approximately 0.5% of the incident photon energy in the soft x-ray regime, corresponding to ~3 eV at the 640 eV Mn L_3-edge [29]. In order to achieve the resolution for Mn L-edge XAS (core-hole lifetime leads to line width of ~0.3 eV at the L_3 absorption edge), the SASE pulse is filtered with a beamline monochromator situated in the experimental hutch ('SXR mono' in Fig. 1). The photon flux is therefore reduced by the grating efficiency of the monochromator in first order (20-35% [29]), and the selection of a narrow bandwidth by the monochromator exit slit.

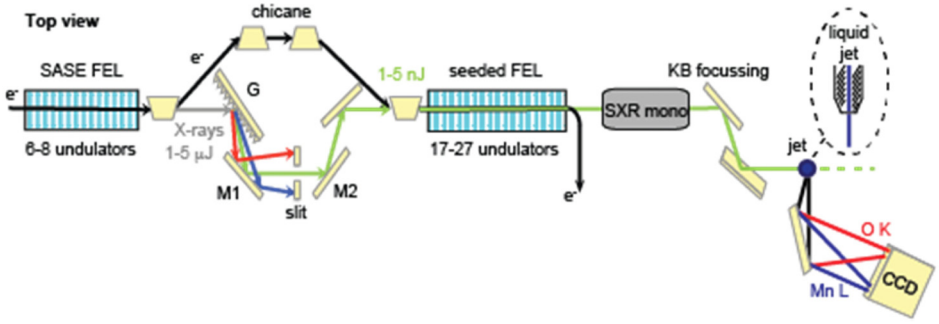

Fig. 1. Schematic of the self-seeded mode setup for L-edge XAS experiments at LCLS. [Scheme adapted from Ratner *et al.*, Phys. Rev. Lett. **114**, 054801 (2015).]

Alternate to SASE operations, LCLS can operate using the self-seeded scheme [34]. In this scheme, a grating monochromator placed upstream after eight undulator sections selects a narrow spectral bandwidth of x-rays that are slightly delayed by the extra pathlength (see Fig. 1). The electrons, passing through a chicane to match that delay, will overlap with these monochromatic photons in the subsequent undulator sections. These monochromatic x-rays then act as a seed for the subsequent amplification in the second set of undulators ('Seeded FEL' in Fig. 1), resulting in a self-seeded beam that does not require the additional beam line monochromator or exit slit as necessary in SASE mode. We therefore tune the beamline monochromator ('SXR mono' in Fig. 1) for 0th order reflection (R~80%) to keep the beam path and open the exit slit of the monochromator, as to not interfere with the x-ray beam. Because the loss in the self-seeding monochromator preceeds the amplification, this approach results in higher brightness than the use of a beamline monochromator that filters out a large

Optics EXPRESS

fraction of the saturated XFEL power. On the other hand, the self-seeding mode can suffer from significant backgrounds, caused by competing SASE growth as well as distortions to the seeded spectrum due to a non-ideal electron beam [39,40]. Using fewer undulator sections improves the spectral quality of seeded beam spectra, but also reduces the final saturation power. As a result, the actual gain of the self-seeding mode compared to SASE mode with a beamline monochromator can vary significantly depending on the desired bandwidth, spectral quality, and photon energy. Hence the number of undulators was varied based on its effect on the XAS spectra of prototypical $MnCl_2$ complex solution.

3. Results and discussion

To perform absorption experiments in the soft x-ray region (250-1000 eV) at an XFEL facility requires an incoming photon energy bandwidth narrower than the SASE bandwidth, and there are three options to achieve this: (a) use of the SASE mode plus a beamline monochromator, (b) use the self-seeded mode without an additional monochromator, or (c) use a combination of the self-seeded beam plus the beamline monochromator to eliminate the background and possibly achieve higher spectral resolution. To estimate their feasibility, multiple questions need to be addressed: How does the self-seeded beam spectral shape vary for a different number of seeded FEL undulators (second undulator set in Fig. 1)? How does the corresponding intensity vary relative to the expected SASE intensity? How does the self-seeded beam spectral shape affect the spectral contrast of the XAS experiment?

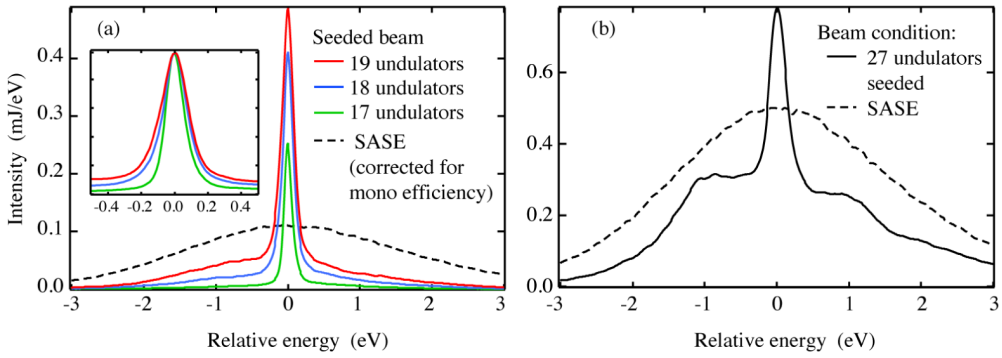

Fig. 2. (a) Average spectra of the self-seeded beam for 17, 18 and 19 undulators plotted with the SASE spectrum corrected for the monochromator efficiency of 0.22 (black dashed). The inset shows the enlargement of the main peak region with all spectra normalized to their maximum value. (b) Comparison of the SASE spectrum (without correction for efficiency) to the seeded beam spectrum for 27 undulators, leading to a strongly increased background.

The spectral shape of the seeded beam spectrum contains three components, which depend on the number of undulators used: the narrow main peak, the SASE background, and a pedestal which, in light of the XAS applications here, can also be qualified as background. The SASE signal grows in the second FEL, where parts of the electron beam are not properly seeded and unseeded amplification increases. The pedestal background is driven by interactions between the seed and a non-ideal electron beam [34,40]. Therefore, the spectrum of the self-seeded beam depends on the number of undulator sections used in the seeded FEL. Figure 2(a) shows the dependence of the intensity and shape of the FEL spectrum on the number of undulator sections used for 17, 18 and 19 sections, and the inset compares their spectral shape normalized to the maximum in a narrow energy range. The narrow seeded peak is accompanied by an asymmetric background originating from the SASE and pedestal signals. When using a larger number of undulators, the intensity in the spectrum increases (see Table 1). At the same time, the fraction of the background (pedestal + SASE) increases from 35% for 17 to 54% for 19 undulators. For 27 undulators, the background signal dominates the total pulse energy with the maximum of the seeded spectrum being around 1.5

Optics EXPRESS

times the maximum of the SASE spectrum (Fig. 2(b), Table 1). The more undulators in the second FEL are used, the stronger is the absolute and relative pedestal background due to the coupling between the growing sideband and the growing seed [40]. The relative increase of the SASE background signal then results from the fact that the seeded signal reaches saturation before the SASE signal does. In future operation, the background contribution may be reduced by improving the suppression of the microbunching instability in the electron beam.

In addition to the change in intensity of the seeded peak and the pedestal or the total background (as well as their ratio), varying the number of undulators can affect the spectral width of the main peak, being a combination of the seeded beam and the pedestal intensity. Hence the spectral resolution is determined by the parameters of the self-seeding, which are defined for each undulator setting. These are fixed for a given electron beam energy and pulse length (see Table 1). The spectral width can be made narrower intentionally either from coherent broadening when shortening the pulse, or by forcing a chirp on the wavelength by putting a quadratic dependence on the electron energy. When using a beamline monochromator in SASE operation, the energy resolution is inversely proportional to the intensity and hence the effective pulse energy as it is given by the exit slit settings, can be optimized to the spectral requirements of each experiment, different from a self-seeded beam.

As shown in Table 1, the pulse energies reached in the seeded beam also depend on the number of undulators used in the seeded FEL. To estimate the pulse energies at the sample for both the self-seeded and the SASE modes of operation, the specific beam line setup has to be taken into account. All of the optical elements of the SXR instrument are employed for both the SASE and the self-seeded modes of operation. Therefore, the difference between the two modes is the incoming pulse energy, the setting of the beamline monochromator to either 0th or 1st order, which leads to different reflectivity properties, as well as the opening of the exit slit (see Table 2). Here, the pulse energies before all optical elements were measured using a gas detector chamber, while the pulse energies after the monochromator exit slit were determined by the gas monitor detector. The front-end enclosure gas detectors (calibrated by the so-called electron loss scan method) are of different type than the so-called "Gas Monitor Detector" (GMD) in the SXR beam line. The GMD is absolutely calibrated, so the mJ pulse energy is measured (not calculated) after the monochromator but in front of the KB optics to less than approximately 10% [32,33].

Table 1. Summary of results of the seeded beam spectra for 17, 18 and 19 undulators. At 640 eV, 1 mJ corresponds to 9.75×10^{12} photons.

Number of undulators	Total intensity (mJ)[a]	Main peak FWHM (meV)	Main peak weight (%)[b]	Background weight (SASE + pedestal) (%)[b]
17	0.081	147	65 ± 4	35 ± 4
18	0.184	207	59 ± 3	41 ± 3
19	0.271	259	46 ± 1	54 ± 1
27	1.311	310	20 ± 5	80 ± 5

[a] The total intensity is determined by the signal measured in the gas detector before any optical elements of the SXR beamline.
[b] The error bars represent the standard deviation of the mean value for different fitting approaches.

The corresponding pulse energies for the three options to achieve high resolution for XAS are compared in Table 2, with option (b) (self-seeded without monochromator) generally leading to highest pulse energies in the sample area. Calculated and experimental pulse energies at the sample, after all optical elements, are compared in the two bottom rows of Table 2. Note that the experimental values were measured before the two KB mirrors and corrected in Table 2 by the reflectivity of these mirrors. No error bars are given for the experimental values due to the unknown dependence of the transmission ratio on the exact

Optics EXPRESS

beam path. However, an overall agreement between the calculated and experimental values is observed.

Table 2. Estimated values of pulse energy before and after the beamline optics at 640 eV for the three different combinations of beam characteristics and monochromator settings. At 640 eV, 1 mJ corresponds to 9.75×10^{12} photons per pulse.

	(a) SASE + monochromator			(b) Seeded			(c) Seeded + monochromator		
Undulators	all			17	18	19	27		
Pulse energy before optics (mJ) [a]	2.0			0.081	0.184	0.271	1.3		
Bandwidth ΔE (meV)[b]	200	400	600	-	-	-	200	400	600
Pulse energy after optics (mJ)	0.003[c]	0.007[c]	0.010[c]	0.009[d]	0.021[d]	0.031[d]	0.007[c]	0.012[c]	0.016[c]
Calculated:									
Measured:			0.012	0.006	0.033				

[a] Experimentally derived values as read by the upstream gas monitor.
[b] The bandwidth is given by the opening of the monochromator exit slit.
[c] Estimated from r_O^6 * r_M * (PE(ΔE)) * c.
[d] Estimated from PE * r_O^7 * c.
Here, PE = incident pulse energy; r_O = reflectivity of the six optical elements, which was determined as 0.79; r_M = reflectivity of the beamline monochromator in 1st order = 0.22; PE(ΔE) = pulse energy of the LCLS spectrum with a band width after the exit slit (ΔE) as given in the third row; and c = clipping of the beam by the mirrors = 0.6.

Beside the difference in pulse energy for the three options, an additional important consideration is the effect of spectral contrast. The background varies with the number of undulators and affects the contrast of the L-edge absorption spectra. To estimate this effect, we utilize a sharp L-edge absorption spectrum that is not broadened by the experimental resolution. In Fig. 3(a), the experimental L-edge partial fluorescence yield spectrum of a $MnCl_2$ solution is shown for a SASE + monochromator setup [24]. The energy bandwidth was set to 300 meV. To obtain the spectrum independent of experimental bandwidth, this measured spectrum was deconvoluted with a Gaussian of FWHM = 300 meV, (see dashed curve in Fig. 3(a)).

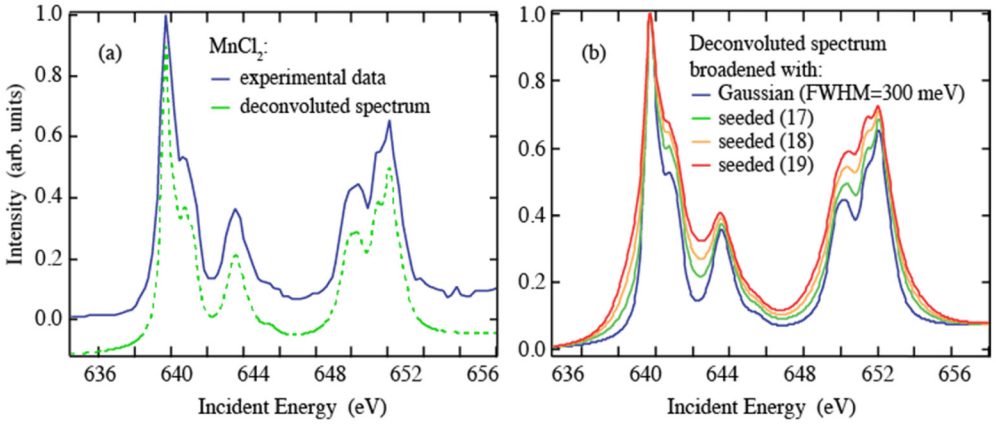

Fig. 3. (a) Experimental fluorescence data of $MnCl_2$ solution [24] together with the experimental broadening deconvoluted spectrum. (b) The deconvoluted spectrum convoluted with a Gaussian of FWHM = 300 meV and the three predicted seeded beam spectra for 17, 18 and 19 undulators (see text, normalized to one at maximum).

Figure 3(b) then shows as a consistency check the convolution of this deconvoluted spectrum with a Gaussian of FWHM = 300 meV, which naturally reproduces the experimental spectrum. We compare this conventionally measured spectrum with the absorption spectrum predicted for XAS measurements in the self-seeded mode in Fig. 1. For this the deconvoluted spectrum was convoluted with the measured FEL spectra (from Fig. 2) when using 17, 18 and 19 undulators in the seeded FEL. All three curves contain all spectral

Optics EXPRESS

features known from the conventionally measured spectrum. With increasing weight of the SASE and pedestal background in the seeded beam spectra for increasing number of undulators in the seeded FEL, we expect the curves to get broader and weak features to smear out slightly. Especially for a large number of undulators, the broad background is predicted to create asymmetries as best seen for low energies around 638.5 eV in Fig. 3(b).

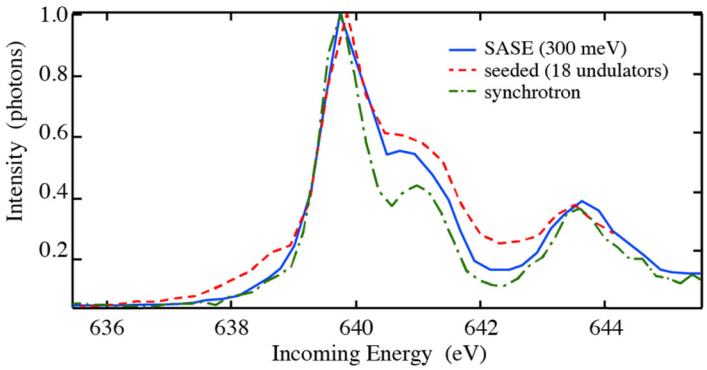

Fig. 4. Comparison of the experimental L_3-edge partial fluorescence spectra of $MnCl_2$ solution (L_3-edge region) for the two modes: SASE + monochromator in 1st order with an energy bandwidth FWHM of 300 meV [24], and self-seeding + monochromator in 0th order. Since the L_3-edge life-time broadening is smaller than the one at the L_2-edge, only the L_3-edge is shown here. For comparison, the synchrotron fluorescence yield spectrum is given.

We could confirm these predictions with a PFY-XAS spectrum measured in self-seeded mode. This is shown in Fig. 4, where the measured Mn L_3 absorption spectra of $MnCl_2$ in solution are compared for the conventional approach with SASE + monochromator with an exit slit bandwidth of 300 meV [24] (i.e. option (a)), and the new self-seeded approach with 18 undulators in the seeded FEL (i.e. option (b)). All spectral features are visible as expected from the predictions in Fig. 3. This emphasizes the feasibility of high resolution XAS in the self-seeded mode of operation with an increase in photon flux. The comparison to a synchrotron fluorescence spectrum further shows that the same spectral shape is reached from both types of facilities. Thus, the reason to use an XFEL is its possibility to provide critical information not accessible at a synchrotron, including dynamics down to fs times as well as obtaining and damage free spectra due to the ultra short life-time of the XFEL pulse [1].

Expecting a corresponding increasing interest in the approach based on self-seeding we now turn to a general discussion of advantages and disadvantages of the three options for measuring XAS at a free-electron laser ((a)-(c), see above). The main advantage of option (a) (SASE + monochromator) is the continuous tunability of the spectral width for a fixed pulse duration. The pulse energy at the sample is inversely proportional to the spectral resolution. The main disadvantage of (a) however, is the loss in pulse energy from both the limited grating throughput and the size of the exit slit, as discussed above (see Table 2).

The main advantage for option (b) (self-seeded without monochromator) is the higher photon flux at the sample by a factor of three as compared to option (a), despite the lower incoming pulse energy (Table 2). In addition the minimum achievable spot size is smaller when working without monochromator.

The main advantage in option (c) (self-seeding with monochromator) is the spectral filtering of the main peak upon suppression of the background, leading to a higher spectral contrast. Due to the suppression of the background signal by the energy selection, a higher number of undulators in the seeding FEL can be used, regardless of the increased background signal. For the same energy resolution as in option (a), this leads to an increase in pulse energy by around a factor of 1.5.

Optics EXPRESS

4. Conclusion and outlook

We have shown that ultrafast monochromatic soft x-ray pulses based on the self-seeding method at LCLS can be directly used without an additional monochromator, to record Mn L-edge absorption spectra. We find that sufficient resolution to discern spectral fine structures can be reached by comparing the partial fluorescence detected XAS spectra of aqueous $MnCl_2$ solutions measured in the self-seeded mode of operation of LCLS with the spectrum measured with the conventional approach based on a monochromator. The spectral shape and intensity of the self-seeded beam depend on the number of undulators used in the seeded FEL, providing some tunability of these parameters to achieve the desired combination of intensity and resolution. Compared to the SASE plus monochromator beam, the self-seeded beam mode resulted in a higher intensity on the sample by approximately a factor of three. With future enhancements in the seeding schemes, this factor is expected to go up. We note that the self-seeding scheme is applicable in a large energy range of 500-1000 eV, which eventually may extend to the operating range 300–1200 eV [34].

Future enhancements in the self-seeding mode can be expected by improving the suppression of the microbunching instability, increasing the seed power, increasing the undulator taper range, reducing the frequency jitter in the LCLS, and with a more stable XFEL source. These improvements will lead to an increase in pulse energy and a suppression of the background signal, giving a stronger spectral contrast in the self-seeded beam spectra. Being able to drive the seeded pulse deeper into lasing saturation will reduce the intensity fluctuations as compared to SASE. Finally, external seeding technologies might help to further improve the signal to background ratio and are under study for the LCLS-II project.

As a consequence, it will widen the setup options using the seeded beam mode and allow more customized setups for future experiments including absorption and RIXS. We anticipate that the self-seeding mode will become the routine choice for soft x-ray spectroscopy at current and future XFEL facilities. The approach presented here will further establish XFEL-based L-edge x-ray spectroscopy as a powerful tool to study the electronic structure of many systems such as metalloenzymes and biomolecules, inorganic complexes, and correlated electron systems. The method should also be applicable to photoemission spectroscopy and, in general, to methods that require a narrow energy bandwidth of the incoming photons. Finally, it will also open up the possibility of doing experiments using nonlinear effects, since these are particularly sensitive to changes in the beam brilliance.

Funding

Human Frontiers Science Project (RGP0063/2013); National Institute of Health (NIH) (GM116423, GM110501, GM55302, P41GM103393); Department of Energy (DOE), Office of Science, Office of Basic Energy Sciences (OBES) (DE-AC02-05CH11231, DE-AC02-76SF00515); Federal Ministry of Education and Research (BMBF) (05K12CB4); Marie Curie FP7-Reintegration-Grants within the 7th European Community Framework Program (PCIG10-GA-2011-297905); Helmholtz Virtual Institute “Dynamic Pathways in Multidimensional Landscapes”.

Portions of this research were carried out on the SXR Instrument at the Linac Coherent Light Source (LCLS), a division of SLAC National Accelerator Laboratory and an Office of Science user facility operated by Stanford University for the U.S. Department of Energy. The SXR Instrument is funded by a consortium whose membership includes the LCLS, Stanford University through the Stanford Institute for Materials Energy Sciences (SIMES), Lawrence Berkeley National Laboratory (LBNL), University of Hamburg through the BMBF priority Program No. FSP 301, and the Center for Free Electron Laser Science (CFEL).

Use of the Linac Coherent Light Source (LCLS), SLAC National Accelerator Laboratory, is supported by the U.S. Department of Energy, Office of Science, Office of Basic Energy

Optics EXPRESS

Sciences under Contract No. DE-AC02-76SF00515. Use of the Stanford Synchrotron Radiation Lightsource, SLAC National Accelerator Laboratory, is supported by the U.S. Department of Energy, Office of Science, Office of Basic Energy Sciences under Contract No. DE-AC02-76SF00515. The SSRL Structural Molecular Biology Program (TK) is supported by the DOE Office of Biological and Environmental Research, and by the National Institutes of Health, National Institute of General Medical Sciences (including P41GM103393). The contents of this publication are solely the responsibility of the authors and do not necessarily represent the official views of NIGMS or NIH.

Acknowledgments

We thank the Helmholtz-Zentrum Berlin for the allocation of synchrotron radiation beamtime.